remote sensing

MDPI

Article

Spatial Heterogeneity and Responses of Wildfire Drivers Across Diverse Climatic Regions in China

Xiaoxiao Feng [1], Huiran Wang [1], Zhiqi Zhang [1,*], Shenggu Yuan [2], Ruofan Jiang [3] and Chaoya Dang [4]

[1] School of Computer Science, Hubei University of Technology, Wuhan 430068, China; fengxx@hbut.edu.cn (X.F.); 102301191@hbut.edu.cn (H.W.)
[2] National Institute of Natural Hazards, Ministry of Emergency Management of China, Beijing 100085, China; shengguyuan@ninhm.ac.cn
[3] Faculty of Geo-Information Science and Earth Observation (ITC), University of Twente, 7500 AE Enschede, The Netherlands; ruofan.jiang@utwente.nl
[4] College of Agriculture, Nanjing Agricultural University, Nanjing 210095, China; dangchaoya@njau.edu.cn
* Correspondence: zzq540@hbut.edu.cn

Highlights

What are the main findings?

- This study reveals the spatiotemporal patterns and driving mechanisms of wildfires in China from 2001 to 2023, with northeastern and southern regions identified as the main hotspots.
- Wildfire drivers exhibit pronounced spatial heterogeneity, with elevation dominating at the national scale and a spatial pattern of topography-dominated and climate-dominated regimes emerging across different climatic regions.

What are the implications of the main findings?

- Incorporating spatial heterogeneity can improve the accuracy and regional applicability of management strategies. The identified nonlinear and threshold responses provide critical information for region-specific wildfire risk assessment and early warning.
- The results support a multi-scale collaborative strategy, in which the national model serves as large-scale monitoring and early warning, while regional models provide the basis for developing fine-tuned fire prevention and control measures tailored to local conditions.

Abstract

Wildfires are a major natural hazard causing extensive ecological damage and endangering human survival. Previous studies on wildfires in China have mostly focused on specific regions or individual drivers, with limited systematic assessments at the long-term and national scales. The spatiotemporal patterns of wildfires and their multiple driving mechanisms under China's diverse climatic regimes remain insufficiently understood. To bridge this gap, we combined MCD64A1 burned area data (2001–2023) with multi-source natural (meteorological, vegetation, and topographic) and anthropogenic factors, using random forest models at both the national and regional scales to examine the spatiotemporal patterns, dominant drivers, and response mechanisms of wildfires in China. The results revealed that: (1) Spatially, wildfires were concentrated in northeastern and southern China, which accounted for 86.20% of the total burned area. Temporally, northern wildfires were primarily a spring-dominated fire regime, with peak activity in March and April, whereas southern wildfires were winter-dominated, peaking in February. (2) At the national scale, elevation was the key topographic factor influencing wildfire occurrence (relative importance = 0.49), with low-elevation and gentle-slope areas being more fire-prone. At the

Check for updates

Academic Editor: Jungho Im

Received: 26 January 2026
Revised: 8 March 2026
Accepted: 25 March 2026
Published: 27 March 2026

Copyright: © 2026 by the authors. Licensee MDPI, Basel, Switzerland. This article is an open access article distributed under the terms and conditions of the Creative Commons Attribution (CC BY) license.

regional scale, the driving factors exhibit spatial differentiation, forming a spatial pattern of topography-dominated and climate-dominated. (3) Partial dependence plot analysis revealed nonlinear and threshold responses. Fire probability increases rapidly when the soil moisture is below 20 mm, while extremely high land surface temperatures in arid regions suppress fire occurrence due to fuel limitations. This study enhances the understanding of spatially heterogeneous wildfire drivers in China and provides a scientific basis for region-specific wildfire prevention and management strategies.

Keywords: wildfire; spatiotemporal pattern; driving factors; random forest; partial dependence plot

1. Introduction

Wildfire is a major hazard to natural ecosystems, possessing significant destructive potential on humanity, society, and the economy [1]. In recent years, extreme and large-scale wildfires have occurred with increasing frequency across the globe [2,3]. Record-breaking events—such as the 2019–2020 fires in southeastern Australia [4], the 2023 wildfire season in Canada [5–7], and the 2025 California fires in the United States [8]—exemplified the emerging global trend toward wildfire extremization [9,10]. These events underscore the importance of wildfire research in ecology and environmental science.

China, as one of the countries with abundant forest resources and frequent wildfire occurrences, is also facing significant wildfire threats. For instance, in 2020, several large forest fires erupted across Sichuan Province, resulting in extensive burned areas and human casualties [11]. In 2023, an unprecedented heatwave and drought affected Chongqing, triggering severe wildfires across multiple districts and counties that posed major challenges to local forest ecosystems and community safety [12]. Beyond their immediate impacts, wildfires can trigger long-term ecological degradation, including declines in soil biodiversity [13], accelerated land degradation, and desertification [14], thereby posing persistent threats to ecosystem stability and human sustainable development. These cascading effects further highlight the necessity of systematically investigating the spatiotemporal dynamics of wildfires and their driving mechanisms, which is essential for providing a scientific basis for more effective wildfire prevention and management policies. However, wildfire research in China has primarily been conducted at the regional or provincial scales, with a focus on fire-prone areas [12,15]. Studies providing comprehensive long-term and large-scale assessments of wildfire patterns remain relatively limited, which indicates that further in-depth investigations are still needed.

The occurrence of wildfires is driven by a combination of natural and anthropogenic factors [4,16]. Among natural factors, meteorological conditions—including high temperatures, drought, and strong winds—directly influence wildfire frequency and intensity by increasing vegetation flammability and fire spread potential [17,18], whereas topographic complexity exerts an indirect effect by modulating fire propagation rates [19]. In terms of anthropogenic factors, human activities—including cultural practices and agricultural burning—often serve as ignition sources and are considered a major driver of the recent increase in wildfire frequency [20,21]. Although numerous studies have examined these factors in different regions of China [22–24], they have typically focused on a limited subset of drivers, lacking systematic assessments of the synergistic effects of multiple natural and anthropogenic factors, thereby restricting a comprehensive understanding of wildfire mechanisms.

Wildfire occurrence and distribution exhibit significant spatial heterogeneity, and the importance of different driving factors varies considerably from one region to another [19,21]. Previous studies have demonstrated that wildfire frequency, intensity, and dominant driving factors differ markedly across regions [6,25,26]. For instance, across climatic zones, wildfires in subtropical regions are generally smaller and less intense than those in cold-temperate regions [27]. In tropical savanna ecosystems, rainfall is the primary determinant of fire occurrence due to sparse vegetation and limited biomass [28]. In Canada, wildfire severity is predominantly controlled by vegetation dryness in most regions, whereas northern regions are more strongly influenced by climate change [6]. These findings indicate that the relative importance of wildfire driving factors varies substantially across regions, and the mechanisms influencing wildfire occurrence and distribution have shifted with changes in spatial environmental conditions. China covers a vast geographical range and encompasses a wide range of climatic zones, which has resulted in significant regional differences in climate, topography, vegetation, and the intensity of human activities [29–31]. These differences give rise to substantial spatial heterogeneity in wildfire frequency, driving mechanisms, and responses across the country. Existing studies have analyzed the major driving factors of wildfires in China at the national scale; however, these analyses are generally conducted at the overall national level, with limited attention given to the spatial heterogeneity of driving factors among different regions [32]. Consequently, examining regional variations in wildfire driving factors and developing targeted models based on these differences are of considerable scientific importance [33,34].

Earlier studies on wildfires predominantly relied on statistical methods—such as frequency ratio [35,36], weight-of-evidence [37], and multi-criteria decision analysis [38]—to quantify the relationships between wildfire occurrence and its driving factors. Although these methods revealed the mechanisms of variables by integrating historical wildfire data and expert knowledge, their reliance on assumptions of independence and linearity limited the ability of statistical models to capture complex nonlinear interactions among variables [39,40]. Machine learning methods can learn complex relationships among variables from high-dimensional, nonlinear, and multi-source heterogeneous data [41]. Compared to traditional approaches, machine learning offers superior capabilities for modeling nonlinear relationships, efficiently handles large-scale datasets, and improves predictive accuracy [42,43]. Among these methods, random forest (RF) has been widely applied in ecological and hazard research due to its robust nonlinear modeling performance and strong resilience to data noise [44–47]. To investigate the driving mechanisms of wildfires, this study used the partial dependence plot (PDP) for model interpretation and analysis of driving factors. PDPs can reflect the marginal effects of individual variables on wildfire response, intuitively illustrate their nonlinear relationships, and further enhance model interpretability [48,49]. Accordingly, RF models combined with feature importance analysis and PDPs were applied in this study to conduct modeling at both the national and regional scales, which provided an in-depth assessment of the mechanisms and spatial variations in the influence of different driving factors.

This study integrated multiple driving factors, including meteorological, topographic, vegetation, and anthropogenic, based on Chinese wildfire data from 2001 to 2023 and constructed an interpretable dual-scale (national and regional scales) analytical framework using RF models, aiming to reveal the spatiotemporal distribution patterns and driving mechanisms of wildfires in China. The main objectives of this study were: (1) to reveal the spatiotemporal distribution patterns of wildfires in China; (2) to quantify the relative importance of different types of driving factors and identify key drivers of wildfires at both the national and regional scales, as well as their regional variations; and (3) to uncover the responses of wildfires to major factors at the national and regional scales using

interpretable machine learning approaches and clarify the heterogeneous mechanisms underlying wildfire occurrence in diverse climatic regions. This study provides a new perspective for understanding the spatial heterogeneity and formation mechanisms of wildfires in China, emphasizes the importance of advancing wildfire research under diverse climatic backgrounds, and informs the development of region-specific, targeted wildfire management strategies.

2. Materials and Methods

2.1. Study Area

The study area covers the whole of China (3°5′N–53°33′N; 73°29′E–135°04′E), with a total land area of approximately 9.63 million km^2. Characterized by a vast geographical extent, complex and diverse topography [50], and rich climatic types, China exhibits a strong spatial heterogeneity in wildfire occurrence. Following previous studies [31,51,52], the whole study area was divided into seven sub-regions: Sub-region 1 (SR1), the temperate and warm-temperate desert of northwest China; Sub-region 2 (SR2), the temperate grassland of Inner Mongolia; Sub-region 3 (SR3), the temperate humid and sub-humid northeast China; Sub-region 4 (SR4), the warm-temperate humid and sub-humid north China; Sub-region 5 (SR5), the subtropical humid central and south China; Sub-region 6 (SR6), the Qinghai–Tibetan Plateau; and Sub-region 7 (SR7), the tropic humid south China (details in Table 1 and Figure 1).

Table 1. Study areas, climate types, topography types, and vegetation types across different climatic sub-regions of China.

Study Areas	Regional Name	Climate Types	Topography Types	Vegetation Types
SR1	The temperate and warm-temperate desert of northwest China	Mid-temperate arid zone	High-altitude plains	Low-density desert shrub plants
SR2	The temperate grassland of Inner Mongolia	Mid-temperate semi-arid zone	High-altitude plains	Meadow and desert grassland
SR3	The temperate humid and sub-humid northeast China	Mid-temperate semi-humid zone	Low-altitude plains and mountains	Coniferous forests, mixed coniferous and broad-leaved forests, grasslands, and food crops
SR4	The warm-temperate humid and sub-humid north China	Warm-temperate semi-humid zone	Low-altitude plains and Loess Plateau	Deciduous broad-leaved forests and food crops
SR5	The subtropical humid central and south China	Northern subtropical humid zone	Low latitude mountains, hills, basins, and plains	High-density evergreen broad-leaved forest and food crops
SR6	The Qinghai–Tibetan Plateau	Plateau temperate semi-arid zone	High-altitude Mountains	High mountain shrubs, alpine meadows, alpine grasslands, and alpine deserts
SR7	The tropic humid south China	Marginal tropical humid zone	Low latitude plains, low mountains, and hills	High-density evergreen broad-leaved forest

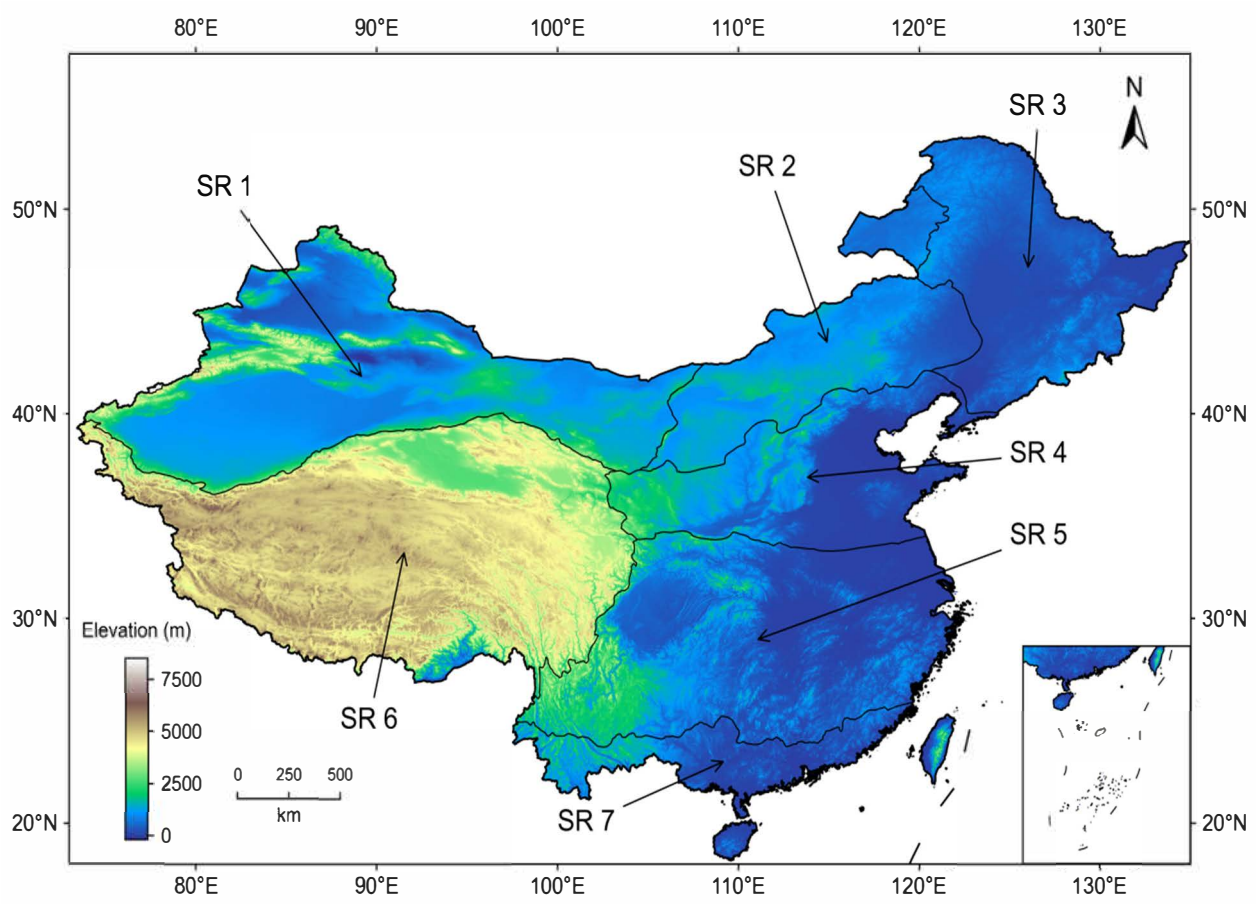


Figure 1. Map of elevation and climatic sub-regions in China.

2.2. Data

2.2.1. Wildfire Data

MODIS burned area product MCD64A1 Collection 6.1 (C6.1) was used in this study [53]. Derived from surface reflectance data acquired by the Terra and Aqua of MODIS, this product constructs a burn-sensitive vegetation index (VI) to create dynamic thresholds that are applied to the composite data. The VI is derived from MODIS shortwave infrared atmospherically corrected surface reflectance bands 5 and 7 with a measure of temporal texture [53]. Collection 6 represents an improvement over the previous MCD64A1 C5.1 and MCD45A1 versions by enhancing sensitivity for detecting small fires and reducing uncertainties in burn date estimation [54]. C6.1 was built on these improvements by incorporating updated input data sources [55]. In recent years, MCD64A1 has been widely adopted in numerous wildfire studies due to its comprehensive spatiotemporal coverage and free accessibility [56]. Its spatial and temporal accuracy has been thoroughly evaluated, and it has been validated as a reliable data source for wildfire research [57,58].

2.2.2. Meteorological Factors

Meteorological conditions are critical external environmental drivers that influence wildfire occurrence, spread and intensity [59]. Seven meteorological variables were selected for this study, including temperature (TEM), precipitation (PRE), relative humidity (RH), wind speed (WS), vapor pressure deficit (VPD), land surface temperature (LST), and Palmer drought severity index (PDSI). TEM and PRE data were obtained from the National Tibetan Plateau Data Center (TPDC), RH data from the ERA5-Land reanalysis of the European Centre for Medium-Range Weather Forecasts (ECMWF), land surface temperature data

from the MODIS products, and other meteorological data from the TerraClimate dataset. The details of these datasets are shown in Table 2.

Table 2. Datasets of wildfire driving factors.

Data Type	Dataset Name	Abbreviation	Spatial Resolution	Data Source
Meteorological	Temperature	TEM	1000 m	https://data.tpdc.ac.cn/
	Precipitation	PRE	1000 m	https://data.tpdc.ac.cn/
	Relative humidity	RH	0.1°	ERA5-LAND (https://cds.climate.copernicus.eu/)
	Wind speed	WS	4638.3 m	TerraClimate (https://www.climatologylab.org)
	Vapor pressure deficit	VPD	4638.3 m	TerraClimate (https://www.climatologylab.org)
	Land surface temperature	LST	1000 m	https://code.earthengine.google.com/
	Palmer drought severity index	PDSI	4638.3 m	TerraClimate (https://www.climatologylab.org)
Vegetation	Normalized difference vegetation index	NDVI	250 m	https://data.tpdc.ac.cn/
	Fractional vegetation cover	FVC	0.05°	https://data.tpdc.ac.cn/
	Soil moisture	SM	4638.3 m	TerraClimate (https://www.climatologylab.org)
	Actual evapotranspiration	AET	4638.3 m	TerraClimate(https://www.climatologylab.org)
Topography	Elevation	ELE	30 m	SRTM (https://code.earthengine.google.com/)
	Slope	Slope	30 m	SRTM (https://code.earthengine.google.com/)
	Aspect	Aspect	30 m	SRTM (https://code.earthengine.google.com/)
	Topographic wetness index	TWI	30 m	SRTM (https://code.earthengine.google.com/)
	Topographic position index	TPI	30 m	SRTM (https://code.earthengine.google.com/)
Anthropogenic	Population density	POP	1000 m	LandScan Global (https://landscan.ornl.gov/)
	Distance to the nearest road	Road	1000 m	https://www.openstreetmap.org/
	Distance to the nearest water	Water	1000 m	https://www.openstreetmap.org/
	Distance to the nearest facility	Facility	1000 m	https://www.openstreetmap.org/

2.2.3. Vegetation Factors

Vegetation factors determine the spatial distribution and combustion potential of fuel loads [60]. The normalized difference vegetation index (NDVI) is an effective indicator for assessing vegetation growth status and potential fuel accumulation. Fractional vegetation cover (FVC) reflects the level and spatial continuity of surface vegetation coverage. To comprehensively evaluate vegetation combustibility, this study also integrated soil moisture (SM) and actual evapotranspiration (AET) into this category for analysis. SM directly affects vegetation water content and fuel drying rate, thereby regulating fuel flammability. AET serves as a key indicator for quantifying vegetation water consumption and drought stress. NDVI and FVC data were both obtained from the TPDC, while SM and AET data were derived from the TerraClimate dataset. The details of these datasets are shown in Table 2.

2.2.4. Topographic Factors

Topographic factors exert a significant influence on wildfire distribution and behavior by regulating local climate, vegetation distribution, and fuel continuity [61]. The topographic wetness index (TWI) reflects the capacity of terrain to accumulate moisture and retain humidity [62]. The topographic position index (TPI) is used to quantify topographic relief and geomorphological patterns, facilitating the exploration of potential impacts of slope position differences on fire risk [63]. Elevation, slope, aspect, TPI, and TWI were all derived from the SRTM Digital Elevation Model (DEM) dataset and computed and downloaded via the Google Earth Engine (GEE) platform [64]. The details of these datasets are shown in Table 2.

2.2.5. Anthropogenic Factors

In addition to the natural factors, human activities are also a crucial factor influencing wildfire occurrence [65]. The anthropogenic factors include population density and the distances from fire ignition points to water bodies, buildings, and roads. Population density data were derived from the LandScan dataset, and the distances were calculated by

Euclidean distances based on OpenStreetMap (OSM) data. The details of these datasets are shown in Table 2.

To evaluate the driving factors derived from multi-source datasets encompassing meteorological, vegetation, topographic, and anthropogenic factors, all variables were resampled and spatially aligned to the 500 m resolution, consistent with the MCD64A1 burned area dataset. This resolution was adopted to maintain consistency with the fire data while balancing the representation of spatial detail and computational efficiency in large-scale modeling [66]. A total of 20 wildfire driving factors were ultimately incorporated into this study, with detailed information (including names, data sources, spatial resolutions, and acquisition platforms) shown in Table 2.

2.3. Methods

2.3.1. Sample Point Construction

Fire samples in this study were generated from the MCD64A1 dataset. Monthly composite data from 2001 to 2023 were downloaded and clipped to the extent of the study area. For the selection of fire samples, only fire points in grassland and forest regions were retained, while those in non-vegetated areas were excluded. By overlaying the fire point locations with the annual MODIS (MCD12Q1.061) land cover product data, those occurring within wetlands, urban and built-up land, agricultural land, and other non-vegetated categories were removed. Both the MCD64A1 fire dataset and the MCD12Q1 land cover dataset were processed and downloaded via the GEE platform.

A binary classification machine learning model was used in this study, where the dependent variable was categorized into two types: 0 (non-fire samples) and 1 (fire samples). The analysis of wildfire driving factors requires a certain proportion of non-fire samples for modeling [67]. Following previous studies [68–70], non-fire samples were created at a 1:1.5 ratio relative to fire samples [71]. The selection of non-fire samples followed three criteria: (1) located in vegetated areas; (2) randomly distributed in time and space; (3) excluded from the 1 km buffer zone around each fire point to minimize spatial autocorrelation.

2.3.2. Random Forest Method

Random forest is an ensemble learning algorithm that constructs a multitude of decision trees and aggregates their outputs to generate predictions [72]. During model training, the bootstrap sampling is employed to draw multiple subsets from the original samples, with each subset used to build an individual decision tree. At each node-splitting step, a random subset of features is selected as candidate variables for optimal partitioning, thereby reducing the correlations among trees. The final prediction result is obtained by aggregating the outputs of all trees [73]. RF has been widely applied in predictive modeling and exhibits excellent performance in variable importance evaluation [74]. In this study, we employed the random forest approach to evaluate the relative importance of wildfire driving factors. The model was implemented in the Python 3.8 environment using the "RandomForestClassifier" module from the Scikit-learn library.

To mitigate model errors, hyperparameter optimization is effective in enhancing model performance and robustness for achieving optimal outputs [75]. Therefore, Grid Search was used for parameter tuning in this study. Specifically, the following parameters were adjusted: the number of decision trees (n_estimators), maximum tree depth (max_depth), minimum number of samples required to split an internal node (min_samples_split), minimum number of samples required at a leaf node (min_samples_leaf), and whether to use bootstrap sampling (bootstrap). The "GridSearchCV" module in Python 3.8 was used to perform five-fold cross-validation on the training dataset, aiming to identify the hyperpa-

rameter combination that maximizes model performance. The optimal hyperparameters are presented in Table 3.

Table 3. Optimal hyperparameters of the random forest model.

Study Areas	Bootstrap	Max_Depth	Min_Samples_Leaf	Min_Samples_Split	N_Estimators
National	True	None	4	10	300
SR1	False	None	1	5	200
SR2	False	10	1	5	300
SR3	False	10	1	2	200
SR4	True	None	4	2	300
SR5	True	10	2	2	100
SR6	True	30	4	10	300
SR7	True	None	4	10	300

2.3.3. Driving Factor Importance Analysis

In this study, the permutation importance (PI) method was used to identify the primary driving factors of wildfire occurrence [76]. This approach assesses feature importance by randomly permuting a specific feature in the trained model and comparing changes in model performance (e.g., out-of-bag error or AUC) before and after the permutation [77]. A significant decline in model accuracy following the permutation of a feature indicates that the feature is critical to the model's prediction. Based on changes in performance, this method evaluates the overall contribution of each variable, enabling a more intuitive measurement of the influence exerted by each wildfire driving factor.

2.3.4. Partial Dependence Plots

This study further analyzed the PDPs to reveal the marginal effects of individual variables on the model prediction results. For machine learning models, PDPs assess the direction and magnitude of a single target feature's impact on prediction results by altering that feature while keeping all other features constant (typically set at their mean values) [78]. This method effectively explains the functional relationship between variables and prediction outcomes and is recognized as one of the commonly used model interpretability tools. Compared with other interpretability methods, PDPs offer the advantage of intuitively illustrating the model's nonlinear responses and threshold effects, providing crucial insights for understanding the mechanisms underlying wildfire occurrence [79]. The corresponding formula is as follows:

$$\hat{f}_{xS}(x_S) = E_{xC}\left[\hat{f}(x_S, x_C)\right] = \int \hat{f}(x_S, x_C) dP(x_C) \quad (1)$$

where $\hat{f}$ is the RF model, x_S represents the target feature variable, x_C denotes the remaining features, $\hat{f}(x_S, x_C)$ is the prediction model, $E_{xC}[\cdot]$ is the expectation over the marginal distribution of x_C, and $dP(x_C)$ is the marginal distribution of the feature x_C.

2.3.5. Model Accuracy Assessment

To evaluate the model accuracy, four commonly used metrics were calculated, including precision, recall, Overall Accuracy (OA), and F1 score. Furthermore, to assess the model's discriminative ability and fitting performance, the area under the receiver operating characteristic curve (AUC) was introduced as a comprehensive indicator. The AUC is a threshold-independent metric that reflects the probability of correctly distinguishing between randomly selected positive and negative samples [80]. An AUC value of 0.5 indicates that the model performs no better than random guessing, while an AUC

approaching 1.0 indicates excellent model performance. In general, a model with an AUC value exceeding 0.75 is considered statistically valid.

To analyze the driving mechanisms of wildfire occurrence and their spatial heterogeneity, RF models were adopted at both the national scale and multiple climatic regional scales. To ensure that the model training process adhered to temporal causality and avoided future information leakage, a time-based five-fold cross-validation strategy was adopted, as presented in Table 4: the training dataset (2001–2019) was divided into five time periods by year, and only the time period earlier than the current validation set was used as training data. This approach ensures that the model training process complies with temporal causality and enhances the reliability of model for future predictions [81,82]. By more authentically simulating the model's predictive performance in future applications, this method strengthens the robustness of the research conclusions [83]. The model was retrained on the entire training dataset (2001–2019), and the final performance was evaluated on an independent test dataset (2020–2023).

Table 4. Time-series cross-validation split.

Fold	Training Years	Validation Years
1	2001–2004	2005–2007
2	2001–2007	2008–2010
3	2001–2010	2011–2013
4	2001–2013	2014–2016
5	2001–2016	2017–2019

3. Results

3.1. Spatiotemporal Patterns of Wildfires in China

3.1.1. Spatial Distribution Pattern

Figure 2 presents the spatial distribution characteristics of 2001–2023 wildfires in China. Wildfires exhibited a spatial clustering characteristic of high occurrence in northeastern and southern China. Among these regions, the wildfire activity was particularly frequent in SR3, ranking as one of the most fire-intensive regions in the country and accounting for about 43.08% of the national total. Over the 23-year period, wildfires occurred multiple times in parts of SR3, with the frequency reaching up to 14 times, which is significantly higher than in other regions. The southern humid regions (SR5 and SR7) followed, ranking as the second most active wildfire regions. By contrast, SR1, SR4, and SR6 experienced fewer wildfires. The latitudinal profile (Figure 2b) further revealed that wildfire in China had distinct peaks in high-latitude areas (45°–55°N) and low-latitude areas (23°–27°N), mainly distributed in the coniferous forests of the northeast mid-temperate semi-humid region (SR3) and the hilly mountainous areas and evergreen broad-leaved forest zones of the southern humid regions (SR5 and SR7).

3.1.2. Temporal Distribution Characteristics

To gain a more comprehensive understanding of the wildfire occurrence patterns in China, this study further analyzed their temporal distribution. In terms of temporal distribution characteristics, the annual distribution of wildfires nationwide exhibited a distinct unimodal pattern, with the high-incidence period concentrated in spring (Figure 3). Among all months, March recorded the largest burned area, averaging 217.38 kha and accounting for 30.22% of the annual total. February and April followed, contributing 16.97% and 14.22%, respectively. By contrast, wildfire activity was extremely weak in summer (June–August), with July accounting for only 0.61% of the annual total, the lowest of the

year. Although winter (November–January) was not a peak period, it still contributed approximately 28.38% of the total burned area.

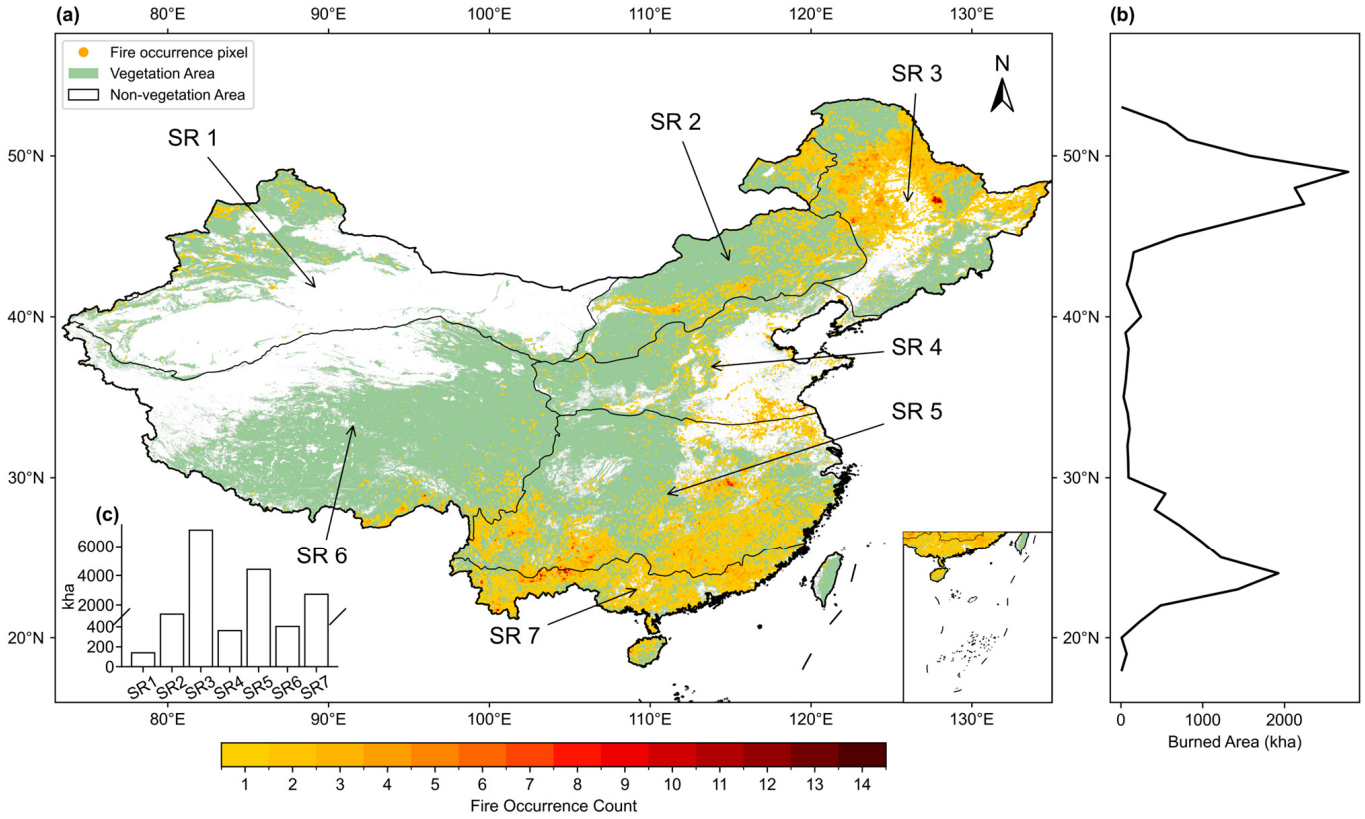


Figure 2. Spatial distribution characteristics of wildfires in China from 2001 to 2023. (**a**) Scatter plot of wildfire occurrence count. Each dot represents a pixel with fire occurrence, and the color intensity indicates the number of fire occurrences recorded at that pixel during 2001–2023. Green indicates vegetated areas, while white indicates non-vegetated areas. The inset in the lower-right corner shows the South China Sea Islands. (**b**) Latitudinal profile distribution of burned area (unit: kha). (**c**) Burned area statistics for the seven climatic sub-regions (unit: kha).

At the regional scale, despite variation in the monthly distribution of wildfire activity across different areas, the spring-dominant pattern constitutes a common characteristic of most regions (Figure 3). For instance, the burn area in SR3 in March accounted for as high as 46.34% of the annual total, with the cumulative proportion in spring exceeding 70.00%, indicating a strong concentration in early spring. SR4 and SR6 also exhibited similar patterns, with spring accounting for 53.38% and 50.74% of their annual wildfires, respectively. Wildfires in SR2 were mainly concentrated in April and May, showing a tendency to shift toward late spring. By contrast, the southern humid regions exhibited a winter-dominant pattern. The proportion of winter wildfires in SR5 reached 57.16%, while that in spring was only 27.57%. The cumulative burned area in SR7 from December to February exceeded half of the annual total, with a single month (February) accounting for 30.40%. This winter concentration is distinctly different from the spring-dominant wildfire pattern in northern regions.

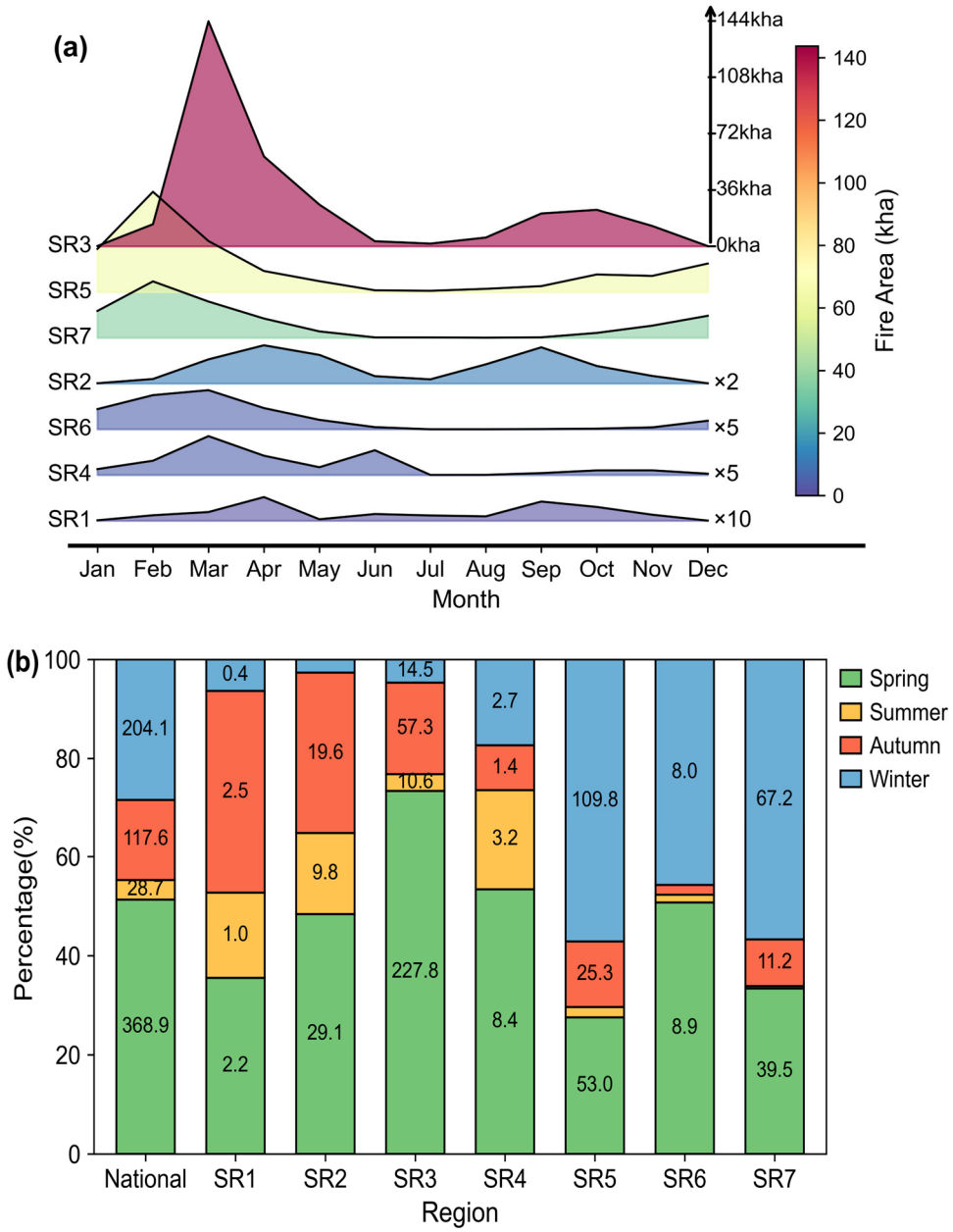


Figure 3. Temporal distribution characteristics of wildfires in China and seven climatic sub-regions from 2001 to 2023. (**a**) Monthly distribution characteristics. (**b**) Seasonal distribution characteristics, with bar values indicating burned area (unit: kha).

3.2. Feature Importance Analysis of Wildfire Driving Mechanisms

3.2.1. Model Performance

Table 5 presents the performance of the RF model across the national scale and different climatic regions. The results indicated that the national-scale AUC value was 0.94. Except for relatively lower AUC values in SR1 (0.81) and SR4 (0.80), the AUC values of all other regions exceeded 0.90 (Table 5), demonstrating that the model performed well at both the national scale and different climatic regions. Regarding other metrics, accuracy and precision were at relatively high levels nationwide and in most regions, indicating that the model performed well in distinguishing between wildfire and non-wildfire samples. The recall in some regions was relatively low (SR1 = 0.48, SR4 = 0.61), which was consistent with the spatial distribution characteristic of sparse wildfire samples in SR1 and SR4 (Figure 2), reflecting that the model's ability to identify wildfires in low-incidence regions

was relatively limited. Overall, the RF model developed in this study exhibited reliable performance across the national scale and different climatic regions, providing support for subsequent wildfire driving mechanisms analysis.

Table 5. Performance metrics of the RF models at national and regional scales.

	ROC-AUC	Accuracy	Precision	Recall	F1 Score
National	0.94	0.89	0.75	0.85	0.80
SR1	0.81	0.79	0.78	0.48	0.59
SR2	0.90	0.84	0.74	0.78	0.76
SR3	0.92	0.85	0.86	0.75	0.80
SR4	0.80	0.86	0.64	0.61	0.63
SR5	0.91	0.85	0.72	0.74	0.73
SR6	0.96	0.89	0.92	0.80	0.86
SR7	0.93	0.84	0.89	0.69	0.78

3.2.2. Feature Importance at the National Scale

Topographic factors contributed the most to wildfires at the national scale (51.1%), significantly higher than meteorological, vegetation, and anthropogenic factors. Among these, elevation exhibited the highest feature importance (0.49), far exceeding other variables, which indicates that topographic height plays a major role in wildfire distribution. For meteorological factors, PDSI (0.06), PRE (0.05), and RH (0.05) ranked among the top, which suggests that moisture condition and hydroclimatic variability are key factors in wildfire occurrence. WS (0.04), LST (0.03), VPD (0.02), and TEM (0.02) had relatively lower contributions but still exerted important effects on fire spread and persistence. Among vegetation factors, SM (0.12) was the most important factor, second only to elevation, which indicates that it indirectly regulates fire risk by affecting vegetation growth and moisture condition. AET (0.03), NDVI (0.02), and FVC (0.02) showed the controlling effects of vegetation quantity and status on wildfires. By contrast, anthropogenic factors had the lowest overall contribution (2.2%), which demonstrates that the natural environment remains the dominant driver of wildfire patterns at the national scale.

3.2.3. Feature Importance at the Regional Scale

Given the heterogeneous climatic and topographic conditions across China, RF models were further constructed for each climatic region to examine regional variations in wildfire drivers. The results revealed substantial spatial differences in feature importance.

Topographic factors played a dominant role in certain regions, particularly in SR3, SR4, and SR6, where the importance of elevation far exceeded that of other variables (all exceeding 0.3), which highlights its high importance in wildfire prediction. Slope also played an important role in SR1 and SR4.

Meteorological factors were the primary factors in most regions, with their influence particularly enhanced in the southern humid regions (SR5, SR7), where factors such as RH, LST, PRE, and PDSI were dominant. Among them, RH exhibited the highest importance in SR7 (0.32), ranking first across all variables.

Vegetation factors showed moderate importance in several regions, particularly in SR5 and SR7. By contrast, anthropogenic factors consistently ranked among the lowest across all climatic regions.

Overall, the importance of wildfire driving factors displays obvious regional differentiation, with distinct topography-dominated and climate-dominated patterns.

Based on the feature ranking results, the top five driving factors are summarized in Table 6. The results indicated that the composition of dominant driving factors varied significantly among different climatic regions. Variables including ELE, RH, LST, and SM

appeared frequently across multiple regions, exhibiting strong spatial consistency and serving as the primary factors triggering wildfire in most areas. By contrast, VPD only appeared in SR2, which reflects its regional specificity.

Table 6. Ranking and relative importance of wildfire driving factors for the national and seven climatic sub-regions (Top 5).

Region	Top 1 Driving Factor (Importance)	Top 2 Driving Factor (Importance)	Top 3 Driving Factor (Importance)	Top 4 Driving Factor (Importance)	Top 5 Driving Factor (Importance)
National	ELE (0.492)	SM (0.120)	PDSI (0.056)	PRE (0.054)	RH (0.052)
SR 1	**ELE(0.160)**	AET (0.084)	Slope (0.078)	**LST(0.071)**	TEM (0.067)
SR 2	**ELE(0.211)**	**SM(0.130)**	TEM (0.096)	**LST(0.087)**	VPD * (0.066)
SR 3	**ELE(0.697)**	**SM(0.077)**	WS (0.051)	PDSI (0.033)	**RH(0.029)**
SR 4	**ELE(0.365)**	**RH(0.094)**	Slope (0.086)	WS (0.083)	TEM (0.060)
SR 5	**RH(0.172)**	**LST(0.131)**	AET (0.120)	PDSI (0.092)	**ELE(0.075)**
SR 6	**ELE(0.315)**	PDSI (0.111)	**SM(0.108)**	PRE (0.075)	WS (0.068)
SR 7	**RH(0.325)**	PRE (0.102)	**SM(0.083)**	**LST(0.078)**	AET (0.063)

Notes: Importance values represent the relative contributions of each factor in the model. Bold indicates common factors; * indicates unique factors.

Regarding different climatic regions, ELE ranked as the top factor in both SR1 and SR2, accompanied by thermal-related variables such as TEM and LST, which indicates that wildfires in arid regions are strongly influenced by topographic and thermal conditions. Meanwhile, the humid regions (SR5 and SR7) were dominated by moisture- and energy-related factors such as RH, PRE, and AET, which suggests that wildfires in southern humid regions are more dependent on the regulation of atmospheric humidity, precipitation, and evapotranspiration.

When comparing the importance ranking of the same factors across different regions, we noticed that the spatial variability became more prominent. ELE consistently ranked first in northern and plateau regions (SR1–SR4, SR6), with the highest importance value of 0.697 in SR3, representing the national maximum. By contrast, ELE's importance declined markedly in southern regions (SR5, SR7), only ranking within or below the top five, indicating that the controlling effect of topography decreases gradually from north to south. RH showed distinct patterns between arid and humid regions, ranking among the top five in humid and semi-humid regions (SR3–SR5, SR7) and serving as a key driver of wildfire occurrence. However, RH was not among the top five factors in arid or semi-arid regions (SR1, SR2, SR6), functioning as a secondary factor. This contrast suggests that RH fluctuations are more likely to trigger wildfires in humid regions, whereas changes in RH in arid regions are insufficient to substantially influence vegetation combustibility. The spatial differentiation was clearly reflected in the heatmap (Figure 4c), where the importance levels of key factors such as ELE, RH, LST, and SM exhibited obvious gradient changes across regions.

3.3. Wildfire Response Characteristics to Key Driving Factors

To gain a deeper understanding of how factors specifically influence wildfire probability, this study employed PDPs derived from RF models to examine the responses of wildfires to key driving factors and their spatial variations. The top five dominant driving factors were analyzed at both the national scale and for seven regions. At the national scale, several factors showed monotonic relationships with wildfire probability (Figures 5 and S1). ELE, PDSI, PRE, slope, and AET displayed negative relationships with wildfire probability, whereas LST showed a positive relationship. Several other variables exhibited nonlinear relationships and threshold effects. RH, WS, TEM, and VPD showed threshold responses, where wildfire probability increased with the variables up to a threshold and declined

beyond it. The response of SM was distinctive: wildfire probability rose sharply within the range of 0–20 mm, then slightly decreased and stabilized when SM exceeds 20 mm.

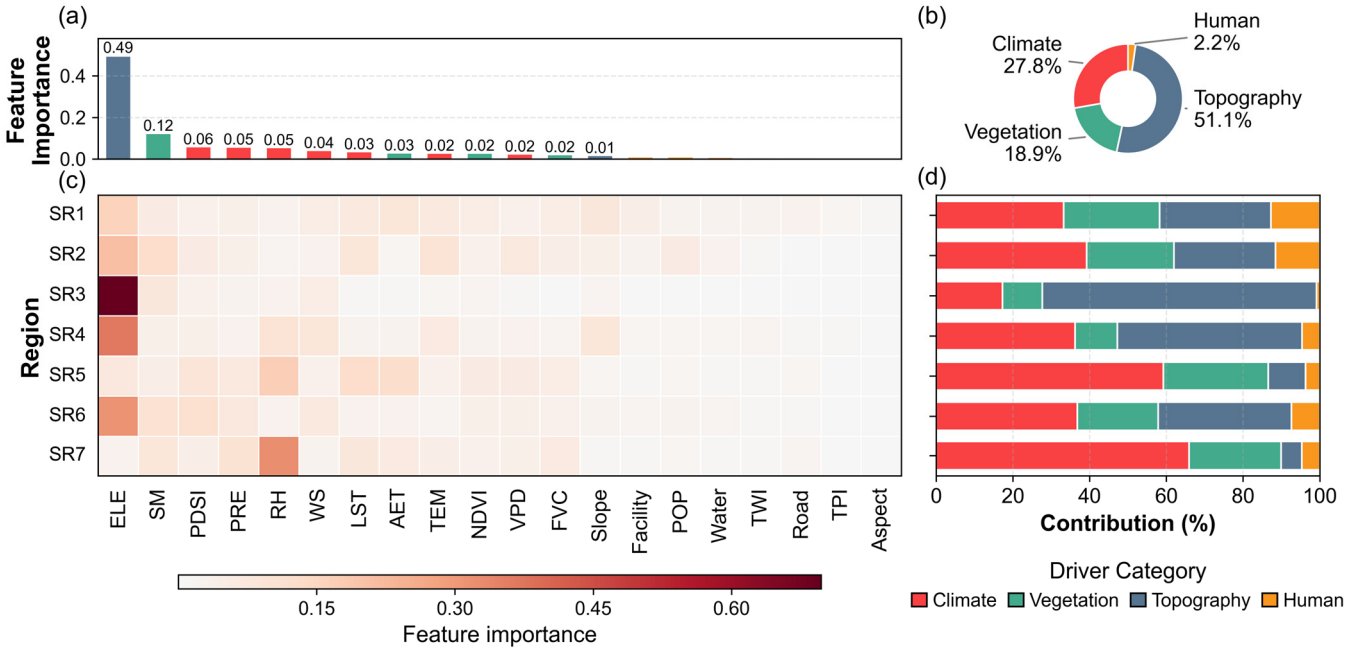


Figure 4. Feature importance of wildfire driving factors. (**a**) Feature importance of driving factors at the national scale. (**b**) Proportional contributions of the four driver categories at the national scale. (**c**) Feature importance of driving factors across different climatic regions. (**d**) Proportional contributions of the four driver categories across different climatic regions.

However, the average response at the national scale conceals regional variations, as the response curves of the same driving factors exhibit spatial heterogeneity across different regions. On the one hand, the response curves of certain factors (e.g., AET, SM, TEM, PRE, PDSI, and VPD) were relatively consistent across regions (Figure S1). Moisture-related factors (AET, PDSI, and PRE) were generally negatively correlated with wildfire probability. TEM and VPD exhibited threshold effects in most regions, though their threshold values were varied. For TEM, the threshold exhibited a distinct north–south gradient: in colder northern regions (e.g., SR1 and SR3), the peak wildfire probability occurs near 0 °C, whereas in central and southern regions (e.g., SR4 and SR5), the threshold increases to approximately 10 °C. For VPD, the critical values in most regions fall within the range of 0.3–1.2 kPa.

On the other hand, other factors (e.g., RH, ELE, LST, slope, and WS) exhibit more pronounced spatial variability (Figure 5). The response curve of RH reflects regional differences in climatic sensitivity: in relatively humid regions (SR3, SR5, and SR7), wildfire probability is highly sensitive to changes in RH and generally displays a threshold effect (critical point around 20%). By contrast, sensitivity to RH is relatively lower in arid regions (SR1, SR2, and SR6), while SR1 and SR4 exhibit monotonic trends in opposite directions.

The response curve of slope is the most diverse, reflecting the differentiated effects of topographic conditions on wildfire occurrence across regions. In SR1, SR2, and SR4, wildfire probability declines sharply in the low slope range; in SR6, it increases monotonically with slope; and in SR3, it continues to decrease. In southern humid regions (SR5, SR7), the response follows a parabolic (initial increase followed by a decrease) pattern, though the overall magnitude of change remains relatively small.

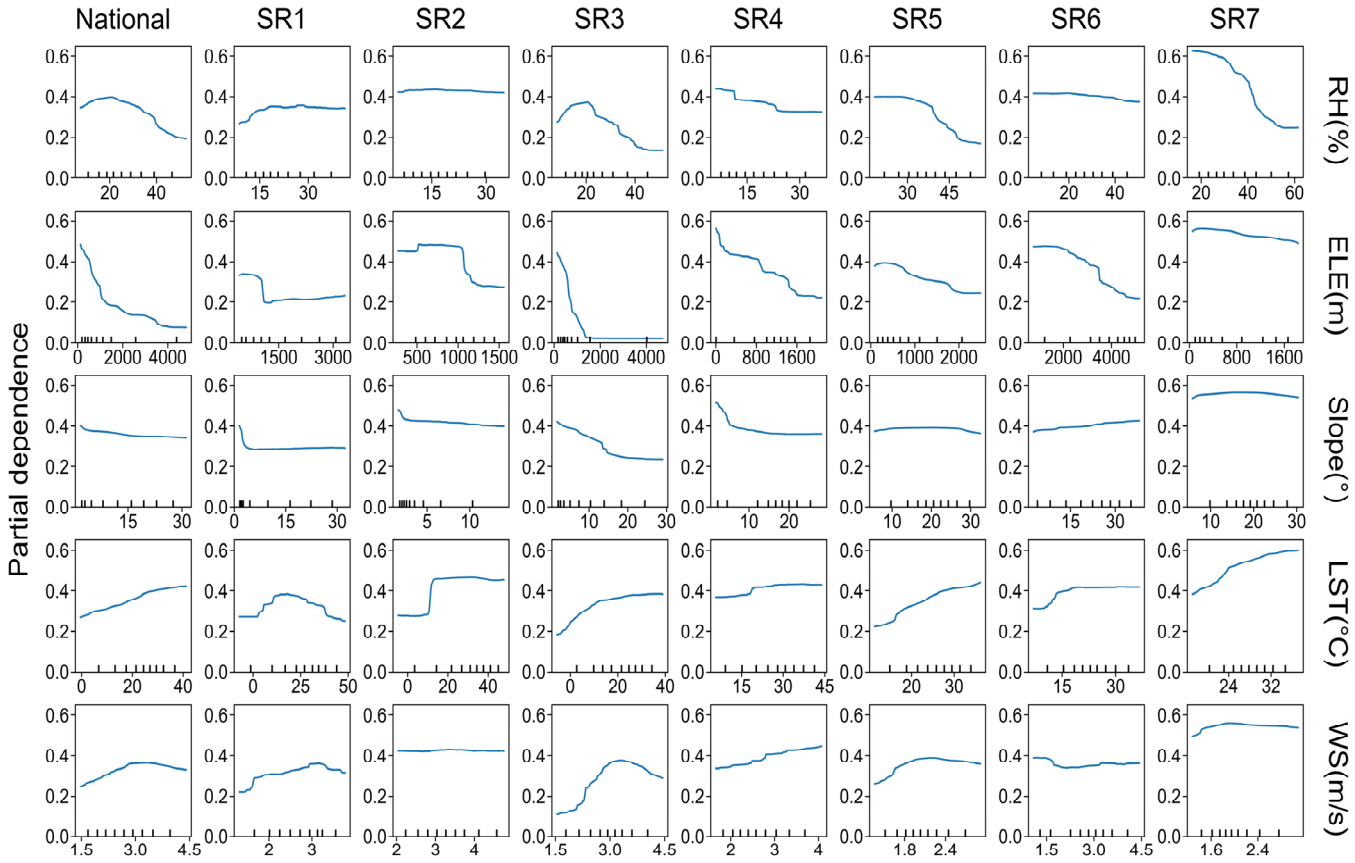


Figure 5. Partial dependence plots illustrating spatially heterogeneous responses of wildfire probability to driving factors across regions.

LST displayed an increasing trend across most regions but exhibited a threshold effect in SR1 (initial increase followed by a decrease). For WS, except for a continuous upward trend in SR4, the response curves in most regions displayed threshold effects with varying critical values: the threshold was approximately 3 m/s in northern regions (SR1, SR3) and around 2 m/s in south regions (SR5, SR7).

In summary, the national scale results reveal that wildfires exhibit threshold effects and nonlinear responses to certain driving factors, while regional results further demonstrate pronounced spatial heterogeneity in these responses.

4. Discussion

4.1. Regional Characteristics of Wildfire Occurrence in China

This study used RF models to analyze the spatiotemporal dynamics of wildfires in China from 2001 to 2023, based on a long-term national fire dataset from the MODIS MCD64A1 product. The observed spatial and seasonal patterns are likely associated with the combined influences of climatic gradients, vegetation distribution, topographic conditions, and human activities.

In northeast China, the mid-temperate semi-humid region exhibits particularly high wildfire activity, with ELE, SM, and WS identified as the primary driving factors (Figure 4, Table 6). The region is dominated by low hills and plains, where extensive coniferous forests provide continuous and abundant fuels for wildfires [84]. Following spring snowmelt, dry combustibles are exposed to dry and windy conditions; concurrently, the soil remains in the thawing stage, and the vegetation has not yet turned green, rendering the region highly susceptible to large-scale fires [85].

Previous studies focusing on northeast China also identified SM and WS as key drivers of wildfires, which is consistent with our findings [86,87]. However, discrepancies exist regarding the role of topographic factors: local-scale studies centered on areas such as the Greater Khingan Mountains have shown that slope, rather than elevation, exerts a stronger influence on wildfire occurrence [88,89]. This inconsistency may be attributed to differences in research scale. For instance, Fang et al. [89] focused on a study area with an elevation range of approximately 800–1500 m. By contrast, our research area covers a much larger spatial scale, with an elevation span exceeding 2000 m. The relatively gentle topographic variability in their study area may have reduced the importance of elevation. Slope, as an indicator reflecting local surface morphology, can more sensitively capture the influence of terrain features on fire spread. This highlights the scale-dependent variation in the importance of topographic factors across various spatial levels.

In the southern humid regions (SR5, SR7), wildfire occurrence is closely associated with moisture conditions. These regions remain warm and humid climates throughout the year, where combustibles are abundant but high humidity suppresses wildfire ignition. During winter, however, the influence of the cold and dry winter monsoon causes periodic declines in relative humidity, temporarily alleviating the moisture-induced suppression of wildfire [20]. PDP analysis clearly indicated a negative correlation between fire probability and RH in SR5 and SR7: lower RH values correspond to higher fire risk. Therefore, the high incidence of winter wildfires in southern China essentially stems from a "flammability window" created by short-term atmospheric drying within an otherwise humid environment. This finding is highly consistent with international studies' conclusions that wildfires in humid ecosystems are driven by moisture fluctuations [90].

4.2. Analysis of Wildfire Driving Mechanism

To better understand the mechanisms underlying wildfire occurrence, this study analyzed the relative contributions of multiple meteorological, topographic, vegetation, and anthropogenic factors. The results revealed significant spatial variability in wildfire driving mechanisms across different climatic regions, showing an overall distribution pattern of topography- and climate-dominated. At the national scale, topographic factors exhibited the highest predictive contribution to wildfire occurrence, with ELE demonstrating substantially higher importance than other variables. The influence of ELE is primarily indirect [91]: it affects wildfire occurrence by regulating climatic and vegetation conditions rather than directly intervening in the combustion process [92]. Owing to China's three-step-staircase topography, elevation comprehensively reflects the gradients of multiple factors, including temperature, precipitation, vegetation types, and even human activities. Low-elevation areas typically feature warmer and drier climates, longer vegetation growing seasons, greater fuel accumulation, and more frequent human activities [93–95], which provide favorable conditions for ignition, resulting in higher overall fire risk. This explains the monotonic decreasing relationship between elevation and fire probability (Figure 5). This finding is also consistent with results from other topographically complex countries, which suggests that topographic factors are the main influences on wildfire occurrence and spatial distribution at the macro scale [96–98].

However, a distinct shift in dominant factors was observed at the regional scale. In mid- and high-latitude regions (SR3, SR4), topographic factors remained highly important. This reflects that within large-scale areas with relatively uniform vegetation and climate conditions, local topography (elevation, slope) becomes a key factor in wildfires by regulating microclimates (wind speed and temperature) and shaping fire spread pathways. In mid-temperate arid and semi-arid regions (SR1, SR2), wildfire driving mechanisms

primarily reflect the combined effects of topography and thermal conditions, which is consistent with the conclusions of previous studies [99–101].

PDP analysis showed that the bell-shaped wildfire response of wildfires to LST in the mid-temperate arid regions reflects the distinctive attributes of regional ecosystems (Figure 5). Unlike most regions, where higher temperatures generally promote wildfire occurrence, extremely high LST in mid-temperate arid zones correlates with decreased fire probability. We hypothesized that in arid environments with extreme water limitations, the hot and dry conditions corresponding to high LST lead to sparse vegetation cover and extremely low fuel loads [102,103]. This created a scenario where climatic conditions are theoretically suitable but fuel availability is limited, which potentially suppressed wildfire occurrence [104]. Such regional variations in the response characteristics of the same variable are not only related to data coverage but also reflect the unique climatic background and vegetation types of different regions.

In southern humid regions (SR5, SR7), meteorological factors become the key drivers of wildfires, with moisture-related variables, particularly RH and PRE, exerting a significantly enhanced influence. This conclusion is consistent with findings from studies focusing on Sichuan and Yunnan Provinces [11,105]. This reaffirms that under conditions of year-round favorable fuel and temperature, fluctuations in moisture conditions can directly alter fuel flammability, persistently resulting in a high sensitivity of wildfire risk to moisture-related factors [39,106].

Notably, the results of this study indicate that anthropogenic factors consistently rank relatively low in importance across all climatic regions, though this does not imply that human activities are unimportant for wildfire occurrence. Previous studies have shown that many wildfire events in China are triggered by human ignitions [107–109]. We speculated that the low importance of anthropogenic factors in this study is more likely a result of spatial scale effects: for the large-scale national and climatic region analysis, the model primarily captures environmental suitability rather than ignition sources. Natural conditions (e.g., meteorological and vegetation factors) constitute the environmental background necessary for wildfire occurrence, while human-induced fire sources act more as triggering factors [110]. Human ignitions can only effectively induce wildfires when natural conditions (e.g., arid climate, flammable vegetation) are conducive. In other words, anthropogenic factors typically exhibit dominance at finer spatial scales, where their explanatory power and importance in wildfire occurrence are substantially enhanced [39,111].

4.3. Management Implications

Based on the aforementioned findings regarding the spatial–temporal patterns and driving mechanisms of wildfires in China, wildfire management and control should adopt a strategy integrating region-specific measures with dynamic adaptability. The detailed suggestions are as follows:

1. Strengthen targeted prevention and seasonal management in high-risk areas. The mid-temperate semi-humid region and southern humid regions are the primary wildfire hotspots in China. Fire monitoring and patrol operations should be reinforced during the spring and winter fire-prone periods, respectively. In the mid-temperate semi-humid region, attention should be paid to fuel management after snowmelt in early spring. Fuel loads can be reduced through mechanical removal and by restricting open-field straw piles. Meanwhile, firebreaks should be established in plots characterized by strong winds and gentle slopes. In the southern humid region, efforts should focus on strengthening understory clearance and the supervision of agricultural burning during the winter peak of litter accumulation.

2. Optimize resource allocation based on different wildfire driving mechanisms. Distinct management strategies should be adopted according to the terrain-dominated and climate-dominated regions identified in this study. In topography-dominated regions (SR3, SR4), firebreaks should be established by taking advantage of natural terrain barriers, and priority should be given to protecting low-altitude, gentle-slope, and fuel-continuous areas with high fire risk. In climate-dominated regions (SR1, SR2, SR5-SR7), meteorological monitoring and early warning should be strengthened, with close attention to abnormal fluctuations in moisture conditions. Preventive measures, such as restricting fire use and implementing forest or mountain access bans, should be implemented in advance.
3. Emphasize the coupling of key drivers' response characteristics with regional background conditions. Management strategies should incorporate the identified response characteristics of key factors. For factors exhibiting threshold effects, critical values should be defined, while for those showing monotonic responses, attention should focus on their high-risk extreme values. By integrating the response characteristics of multiple drivers with regional climatic and topographic contexts, a differentiated wildfire prevention and early-warning system that is more targeted and dynamically adaptive can be developed.

4.4. Limitations and Future Perspectives

Although this study systematically analyzed the driving mechanisms of wildfires in China and provided valuable insights at both the national and regional scales, several limitations remain. First, regarding the datasets, most of the data used in this study were derived from remote sensing products and reanalysis datasets. The quality and accuracy of these datasets may be affected by certain uncertainties, and some datasets have relatively low spatial resolution. Future studies could further develop higher-resolution and higher-quality open datasets to provide more accurate and reliable information for wildfire analysis. In addition, regarding the representation of anthropogenic factors, this study primarily relied on static or low-frequency datasets (e.g., population density and the distance from ignition points to roads). While these variables are effective in revealing the macro-spatial patterns of human influence, they have limited capacity to characterize highly dynamic human activities (e.g., seasonal agricultural production and specific festival events) as well as broader socioeconomic factors. Future studies incorporating high-frequency data such as farming activities, holiday firework use, tourist mobility, and nighttime light data could provide more precise assessments of the role of human activities in wildfire occurrence.

Second, although a 1 km buffer was applied to reduce spatial autocorrelation between fire and non-fire samples, residual spatial autocorrelation may still exist due to the spatial continuity of environmental drivers. Future studies could further adopt modeling frameworks that explicitly account for spatial autocorrelation. In addition, in some sub-regions with relatively limited fire samples, model performance was relatively moderate, which may introduce additional uncertainty into the estimation of driver importance. Therefore, the interpretation of the results for these regions should be treated with caution.

Third, it should be emphasized that the feature importance derived from the RF model reflects the relative contribution of variables to predictive performance rather than direct causal mechanisms. Similarly, the thresholds identified from the PDP analysis represent model-derived response patterns and should not be interpreted as universal ecological breakpoints.

Finally, this study primarily focused on the spatial heterogeneity of wildfire driving mechanisms across different climatic regions. Future studies could further investigate the temporal evolution of wildfire driving mechanisms, which may reveal potential shifts

in driver importance under ongoing climate change. Moreover, the interactions among drivers require deeper exploration, as wildfire occurrence may result from the synergistic effects of multiple interacting variables. Future studies could adopt modeling approaches capable of revealing interaction effects, further quantifying the synergistic influence of compound extreme events on fire activity.

5. Conclusions

This study systematically revealed the spatiotemporal patterns, key driving factors, and response mechanisms of wildfires across China from 2001 to 2023. The main conclusions are as follows:

1. Wildfires in China exhibit pronounced spatial and temporal clustering. Spatially, the northeastern and southern regions represent the primary wildfire hotspots (accounting for 86.20% of the national total), with the northeastern mid-temperate semi-humid region (SR3) serving as the core hotspot. Temporally, a spatial contrast is observed between the Northern Spring Fire regime (mainly concentrated in March–April) and the Southern Winter Fire regime (mainly concentrated in February).
2. The driving mechanisms of wildfires exhibit pronounced spatial heterogeneity. At the national scale, elevation is the key topographic factor that primarily drives wildfire distribution, with fires more likely to occur in low-altitude and gentle-slope areas. At the regional scale, the driving mechanisms display a distribution pattern characterized by topography-dominated regions (mainly influenced by ELE) and climate-dominated regions (mainly influenced by RH). Specifically, the influence of ELE gradually weakens from north to south, whereas the influence of relative humidity increases markedly from dry to humid zones.
3. The nonlinear responses of primary driving factors reveal the threshold characteristics of fire probability variation. Wildfire probability rises sharply when SM is within the low moisture content range (0–20 mm), and RH exhibits a threshold effect at around 20%. Furthermore, the responses display significant regional variations. For instance, the bell-shaped response of LST is unique to the arid region (SR1), where extremely high land surface temperatures tend to suppress fire occurrence. The TEM threshold also shows a north–south gradient, being lower in the north and higher in the south.
4. The RF model developed in this study demonstrates reliable performance. Model evaluations across different spatial scales indicate that the national model exhibits high predictive stability and robustness (AUC = 0.94), while the regional models maintain high accuracy and better reveal regionally differentiated driving mechanisms (AUC = $0.81 - 0.93$). The results support a multi-scale collaborative strategy in which the national model serves for large-scale monitoring and early warning while regional models provide the basis for developing fine-tuned fire prevention and control measures tailored to local conditions.

This research elucidates the spatiotemporal distribution characteristics of wildfires and identifies the primary drivers influencing their occurrence, highlighting the pronounced spatial heterogeneity of driving mechanisms in China. These insights provide a scientific foundation for region-specific wildfire prevention and management strategies.

Supplementary Materials: The following supporting information can be downloaded at: https://www.mdpi.com/article/10.3390/rs18071007/s1, Figure S1: Partial dependence plots illustrating relatively consistent responses of wildfire probability to driving factors across regions.

Author Contributions: Conceptualization, X.F.; methodology, X.F. and H.W.; investigation, H.W.; resources, Z.Z. and S.Y.; data curation, H.W.; writing—original draft preparation, X.F. and H.W.; writing—review and editing, X.F., H.W., R.J. and C.D.; supervision, Z.Z., S.Y., R.J. and C.D.; project

administration, X.F.; funding acquisition, Z.Z. All authors have read and agreed to the published version of the manuscript.

Funding: This study was financially supported by research grants from the National Institute of Natural Hazards, Ministry of Emergency Management of China (Grant Number: ZDJ2025-42), and Scientific Research Foundation for Doctoral Program of Hubei University of Technology, China (No. XJ2022005101).

Data Availability Statement: The datasets analyzed in this study were derived from publicly available sources. Burned area data were obtained from the MODIS MCD64A1 Version 6.1 product (MODIS/061/MCD64A1) provided by the NASA LP DAAC (https://lpdaac.usgs.gov/products/mcd64a1v061/, accessed on 12 January 2025). Meteorological variables, including temperature (TEM) and precipitation (PRE), were acquired from the National Tibetan Plateau Data Center (https://data.tpdc.ac.cn/, accessed on 28 February 2025). Relative humidity (RH) data were obtained from the ERA5-Land reanalysis dataset (https://cds.climate.copernicus.eu/, accessed on 28 February 2025). Wind speed (WS), vapor pressure deficit (VPD), Palmer drought severity index (PDSI), soil moisture (SM), and actual evapotranspiration (AET) were retrieved from the TerraClimate dataset (https://www.climatologylab.org/terraclimate.html, accessed on 15 March 2025). Land surface temperature (LST) data were accessed via Google Earth Engine (https://code.earthengine.google.com/, accessed on 08 April 2025). Vegetation indices, including the normalized difference vegetation index (NDVI) and fractional vegetation cover (FVC), were obtained from the National Tibetan Plateau Data Center (https://data.tpdc.ac.cn/, accessed on 04 April 2025). Topographic variables, including elevation, slope, aspect, topographic wetness index (TWI), and topographic position index (TPI), were derived from the SRTM DEM dataset available through Google Earth Engine (https://developers.google.com/earth-engine/datasets/catalog/USGS_SRTMGL1_003, accessed on 22 April 2025). Anthropogenic variables, including population density, were obtained from LandScan Global (https://landscan.ornl.gov/, accessed on 15 May 2025), while road, water, and facility layers were derived from OpenStreetMap (https://www.openstreetmap.org/, accessed on 15 May 2025).

Conflicts of Interest: The authors declare no conflicts of interest.

References

1. Turco, M.; Herrera, S.; Tourigny, E.; Chuvieco, E.; Provenzale, A. A comparison of remotely-sensed and inventory datasets for burned area in Mediterranean Europe. *Int. J. Appl. Earth Obs. Geoinf.* **2019**, *82*, 101887. [CrossRef]
2. Kitzberger, T.; Tiribelli, F.; Barberá, I.; Gowda, J.H.; Morales, J.M.; Zalazar, L.; Paritsis, J. Projections of fire probability and ecosystem vulnerability under 21st century climate across a trans-Andean productivity gradient in Patagonia. *Sci. Total Environ.* **2022**, *839*, 156303. [CrossRef]
3. Wang, X.; Swystun, T.; Flannigan, M.D. Future wildfire extent and frequency determined by the longest fire-conducive weather spell. *Sci. Total Environ.* **2022**, *830*, 154752. [CrossRef] [PubMed]
4. Abdollahi, A.; Pradhan, B. Explainable artificial intelligence (XAI) for interpreting the contributing factors feed into the wildfire susceptibility prediction model. *Sci. Total Environ.* **2023**, *879*, 163004. [CrossRef]
5. Jain, P.; Barber, Q.E.; Taylor, S.W.; Whitman, E.; Castellanos Acuna, D.; Boulanger, Y.; Chavardes, R.D.; Chen, J.; Englefield, P.; Flannigan, M.; et al. Drivers and Impacts of the Record-Breaking 2023 Wildfire Season in Canada. *Nat. Commun.* **2024**, *15*, 6764. [CrossRef] [PubMed]
6. Wang, W.; Wang, X.; Flannigan, M.D.; Guindon, L.; Swystun, T.; Castellanos-Acuna, D.; Wu, W.; Wang, G. Canadian forests are more conducive to high-severity fires in recent decades. *Science* **2025**, *387*, 91–97. [CrossRef] [PubMed]
7. Byrne, B.; Liu, J.; Bowman, K.W.; Pascolini-Campbell, M.; Chatterjee, A.; Pandey, S.; Miyazaki, K.; van der Werf, G.R.; Wunch, D.; Wennberg, P.O.; et al. Carbon emissions from the 2023 Canadian wildfires. *Nature* **2024**, *633*, 835–839. [CrossRef]
8. Qiu, M.; Chen, D.; Kelp, M.; Li, J.; Huang, G.; Yazdi, M.D. The rising threats of wildland-urban interface fires in the era of climate change: The Los Angeles 2025 fires. *Innovation* **2025**, *6*, 100835. [CrossRef]
9. Jain, P.; Castellanos-Acuna, D.; Coogan, S.C.; Abatzoglou, J.T.; Flannigan, M.D. Observed increases in extreme fire weather driven by atmospheric humidity and temperature. *Nat. Clim. Change* **2022**, *12*, 63–70. [CrossRef]
10. Abatzoglou, J.T.; Kolden, C.A.; Cullen, A.C.; Sadegh, M.; Williams, E.L.; Turco, M.; Jones, M.W. Climate change has increased the odds of extreme regional forest fire years globally. *Nat. Commun.* **2025**, *16*, 6390. [CrossRef]
11. Tian, Y.; Wu, Z.; Li, M.; Wang, B.; Zhang, X. Forest Fire Spread Monitoring and Vegetation Dynamics Detection Based on Multi-Source Remote Sensing Images. *Remote Sens.* **2022**, *14*, 4431. [CrossRef]

12. Gutiérrez Rodríguez, L.; He, Y.; Sun, M.; Yao, Y.; de Dios, V.R. Summer Compound Drought-Heat Extremes Amplify Fire-Weather Risk and Burned Area beyond Historical Thresholds in Chongqing Region, Subtropical China. *Fire* **2023**, *6*, 346. [CrossRef]
13. Mantoni, C.; Di Musciano, M.; Fattorini, S. Use of microarthropods to evaluate the impact of fire on soil biological quality. *J. Environ. Manag.* **2020**, *266*, 110624. [CrossRef]
14. Sayad, Y.O.; Mousannif, H.; Al Moatassime, H. Predictive modeling of wildfires: A new dataset and machine learning approach. *Fire Saf. J.* **2019**, *104*, 130–146. [CrossRef]
15. Yue, W.; Ren, C.; Liang, Y.; Liang, J.; Lin, X.; Yin, A.; Wei, Z. Assessment of Wildfire Susceptibility and Wildfire Threats to Ecological Environment and Urban Development Based on GIS and Multi-Source Data: A Case Study of Guilin, China. *Remote Sens.* **2023**, *15*, 2659. [CrossRef]
16. Jones, M.W.; Abatzoglou, J.T.; Veraverbeke, S.; Andela, N.; Lasslop, G.; Forkel, M.; Smith, A.J.P.; Burton, C.; Betts, R.A.; van der Werf, G.R.; et al. Global and Regional Trends and Drivers of Fire Under Climate Change. *Rev. Geophys.* **2022**, *60*, e2020RG000726. [CrossRef]
17. Pausas, J.G.; Keeley, J.E. Wildfires and global change. *Front. Ecol. Environ.* **2021**, *19*, 387–395. [CrossRef]
18. Akıncı, H.A.; Akıncı, H. Machine learning based forest fire susceptibility assessment of Manavgat district (Antalya), Turkey. *Earth Sci. Inform.* **2023**, *16*, 397–414. [CrossRef]
19. Carcaillet, C.; Boulley, B.; Carcaillet, F. Once upon a time biomass burning in the western Alps: Nesting effects of climate and local drivers on long-term subalpine fires. *For. Ecosyst.* **2022**, *9*, 100024. [CrossRef]
20. Fang, K.; Yao, Q.; Guo, Z.; Zheng, B.; Du, J.; Qi, F.; Yan, P.; Li, J.; Ou, T.; Liu, J.; et al. ENSO modulates wildfire activity in China. *Nat. Commun.* **2021**, *12*, 1764. [CrossRef] [PubMed]
21. Zerbe, K.; Cook, T.; Vulcano, A. Multivariate spatial regressions help explain wildfire hot spot intensities in Washington, USA. *Nat. Hazards Res.* **2024**, *4*, 288–294. [CrossRef]
22. Wu, Z.; Li, M.; Wang, B.; Tian, Y.; Quan, Y.; Liu, J. Analysis of Factors Related to Forest Fires in Different Forest Ecosystems in China. *Forests* **2022**, *13*, 1021. [CrossRef]
23. Wei, P.; Lamont, B.; He, T.; Xue, W.; Wang, P.C.; Song, W.; Zhang, R.; Keyhani, A.B.; Zhao, S.; Lu, W.; et al. Vegetation−fire feedbacks increase subtropical wildfire risk in scrubland and reduce it in forests. *J. Environ. Manag.* **2024**, *351*, 119726. [CrossRef]
24. Xing, H.; Fang, K.; Yao, Q.; Zhou, F.; Ou, T.; Liu, J.; Zhou, S.; Jiang, S.; Chen, Y.; Bai, M.; et al. Impacts of changes in climate extremes on wildfire occurrences in China. *Ecol. Indic.* **2023**, *157*, 111288. [CrossRef]
25. Zhao, H.; Zhang, Z.; Wang, X.; Zhen, S.; Zhang, H.; Bu, Z.-J.; Zhao, J.; Guo, X.; Wei, K.; Dong, L. Future enhanced threshold effects of wildfire drivers could increase burned areas in northern mid- and high latitudes. *Commun. Earth Environ.* **2025**, *6*, 224. [CrossRef]
26. Chen, G.; Qiu, M.; Wang, P.; Zhang, Y.; Shindell, D.; Zhang, H. Continuous wildfires threaten public and ecosystem health under climate change across continents. *Front. Environ. Sci. Eng.* **2024**, *18*, 130. [CrossRef]
27. Guo, L.; Li, S.; Wu, Z.; Parsons, R.A.; Lin, S.; Wu, B.; Sun, L. Assessing spatial patterns and drivers of burn severity in subtropical forests in Southern China based on Landsat 8. *For. Ecol. Manag.* **2022**, *524*, 120515. [CrossRef]
28. Richardson, D.; Black, A.S.; Irving, D.; Matear, R.J.; Monselesan, D.P.; Risbey, J.S.; Squire, D.T.; Tozer, C.R. Global increase in wildfire potential from compound fire weather and drought. *Npj Clim. Atmos. Sci.* **2022**, *5*, 23. [CrossRef]
29. Ding, Y.; Xu, J.; Wang, X.; Cai, H.; Zhou, Z.; Sun, Y.; Shi, H. Propagation of meteorological to hydrological drought for different climate regions in China. *J. Environ. Manag.* **2021**, *283*, 111980. [CrossRef]
30. Chen, H.; Wang, G.; Sun, J.; Guo, L.; Song, C.; Sun, X. Spatial and temporal dynamics of plant water source distribution in China. *Remote Sens. Environ.* **2025**, *328*, 114843. [CrossRef]
31. Ding, Y.; Lu, Z.; Wu, L.; Zhou, L.; Ao, T.; Xu, J.; Wei, R. Evaluating the spatiotemporal dynamics of driving factors for multiple drought types in different climate regions of China. *J. Hydrol.* **2024**, *640*, 131710. [CrossRef]
32. Zhang, G.; Zhang, L.; Li, X.; Feng, X.; Wang, Y.; Guo, J.; Li, P.; Wei, X. Spatiotemporal evolution characteristics and driving mechanisms of wildfires in China under the context of climate change and human activities. *Ecol. Indic.* **2025**, *176*, 113694. [CrossRef]
33. Katagis, T.; Gitas, I.Z.; Mitri, G.H. An Object-Based Approach for Fire History Reconstruction by Using Three Generations of Landsat Sensors. *Remote Sens.* **2014**, *6*, 5480–5496. [CrossRef]
34. Guo, L.; Wu, Z.; Li, S.; Xie, G. The relative impacts of vegetation, topography and weather on landscape patterns of burn severity in subtropical forests of southern China. *J. Environ. Manag.* **2024**, *351*, 119733. [CrossRef]
35. de Santana, R.O.; Delgado, R.C.; Schiavetti, A. Modeling susceptibility to forest fires in the Central Corridor of the Atlantic Forest using the frequency ratio method. *J. Environ. Manag.* **2021**, *296*, 113343. [CrossRef] [PubMed]
36. Pourtaghi, Z.S.; Pourghasemi, H.R.; Rossi, M. Forest fire susceptibility mapping in the Minudasht forests, Golestan province, Iran. *Environ. Earth Sci.* **2015**, *73*, 1515–1533. [CrossRef]
37. Ye, J.; Wu, M.; Deng, Z.; Xu, S.; Zhou, R.; Clarke, K.C. Modeling the spatial patterns of human wildfire ignition in Yunnan province, China. *Appl. Geogr.* **2017**, *89*, 150–162. [CrossRef]

38. Sari, F. Forest fire susceptibility mapping via multi-criteria decision analysis techniques for Mugla, Turkey: A comparative analysis of VIKOR and TOPSIS. *For. Ecol. Manag.* **2021**, *480*, 118644. [CrossRef]
39. Li, W.; Xu, Q.; Yi, J.; Liu, J. Predictive model of spatial scale of forest fire driving factors: A case study of Yunnan Province, China. *Sci. Rep.* **2022**, *12*, 19029. [CrossRef]
40. Xu, Z.; Li, J.; Cheng, S.; Rui, X.; Zhao, Y.; He, H.; Guan, H.; Sharma, A.; Erxleben, M.; Chang, R.; et al. Deep learning for wildfire risk prediction: Integrating remote sensing and environmental data. *ISPRS J. Photogramm. Remote Sens.* **2025**, *227*, 632–677. [CrossRef]
41. Hong, T.; Yim, S.H.L.; Heo, Y. Interpreting complex relationships between urban and meteorological factors and street-level urban heat islands: Application of random forest and SHAP method. *Sustain. Cities Soc.* **2025**, *126*, 106353. [CrossRef]
42. Eskandari, S.; Pourghasemi, H.R.; Tiefenbacher, J.P. Fire-susceptibility mapping in the natural areas of Iran using new and ensemble data-mining models. *Environ. Sci. Pollut. Res.* **2021**, *28*, 47395–47406. [CrossRef]
43. Singha, C.; Swain, K.C.; Moghimi, A.; Foroughnia, F.; Swain, S.K. Integrating geospatial, remote sensing, and machine learning for climate-induced forest fire susceptibility mapping in Similipal Tiger Reserve, India. *For. Ecol. Manag.* **2024**, *555*, 121729. [CrossRef]
44. Lin, A.; Wu, H.; Luo, W.; Fan, K.; Liu, H. How does urban heat island differ across urban functional zones? Insights from 2D/3D urban morphology using geospatial big data. *Urban Clim.* **2024**, *53*, 101787. [CrossRef]
45. Xu, H.; Chen, H.W.; Chen, D.; Wang, Y.; Yue, X.; He, B.; Guo, L.; Yuan, W.; Zhong, Z.; Huang, L.; et al. Global patterns and drivers of post-fire vegetation productivity recovery. *Nat. Geosci.* **2024**, *17*, 874–881. [CrossRef]
46. Guo, W.; Huang, S.; Huang, Q.; Leng, G.; Mu, Z.; Han, Z.; Wei, X.; She, D.; Wang, H.; Wang, Z.; et al. Drought trigger thresholds for different levels of vegetation loss in China and their dynamics. *Agric. For. Meteorol.* **2023**, *331*, 109349. [CrossRef]
47. Quintano, C.; Fernández-Manso, A.; Roberts, D.A. Enhanced burn severity estimation using fine resolution ET and MESMA fraction images with machine learning algorithm. *Remote Sens. Environ.* **2020**, *244*, 111815. [CrossRef]
48. Wang, W.; Zhao, F.; Wang, Y.; Huang, X.; Ye, J. Seasonal differences in the spatial patterns of wildfire drivers and susceptibility in the southwest mountains of China. *Sci. Total Environ.* **2023**, *869*, 161782. [CrossRef]
49. Sun, D.; Ding, Y.; Wen, H.; Zhang, F.; Zhang, J.; Gu, Q.; Zhang, J. SHAP-PDP hybrid interpretation of decision-making mechanism of machine learning-based landslide susceptibility mapping: A case study at Wushan District, China. *Egypt. J. Remote Sens. Space Sci.* **2024**, *27*, 508–523. [CrossRef]
50. Zhao, J.; Chen, C. *Chinese Geography*; Higher Education Press: Beijing, China, 1999.
51. Yao, N.; Li, Y.; Lei, T.; Peng, L. Drought evolution, severity and trends in mainland China over 1961-2013. *Sci. Total Environ.* **2018**, *616–617*, 73–89. [CrossRef]
52. Zhao, S.-Q. A new scheme for comprehensive physical regionalization in China. *Acta Geogr. Sin.* **1983**, *38*, 1–10. [CrossRef]
53. Giglio, L.; Boschetti, L.; Roy, D.P.; Humber, M.L.; Justice, C.O. The Collection 6 MODIS burned area mapping algorithm and product. *Remote Sens. Environ.* **2018**, *217*, 72–85. [CrossRef] [PubMed]
54. Humber, M.L.; Boschetti, L.; Giglio, L.; Justice, C.O. Spatial and temporal intercomparison of four global burned area products. *Int. J. Digit. Earth* **2019**, *12*, 460–484. [CrossRef]
55. Giglio, L.; Boschetti, L.; Roy, D.; Hoffmann, A.A.; Humber, M.; Hall, J.V. *Collection 6 Modis Burned Area Product User's Guide*; Version 1.0; NASA EOSDIS Land Processes DAAC: Sioux Falls, SD, USA, 2016; pp. 11–27.
56. Zhang, G.; Wang, M.; Liu, K. Forest Fire Susceptibility Modeling Using a Convolutional Neural Network for Yunnan Province of China. *Int. J. Disaster Risk Sci.* **2019**, *10*, 386–403. [CrossRef]
57. Katagis, T.; Gitas, I.Z. Assessing the Accuracy of MODIS MCD64A1 C6 and FireCCI51 Burned Area Products in Mediterranean Ecosystems. *Remote Sens.* **2022**, *14*, 602. [CrossRef]
58. Katagis, T.; Gitas, I.Z. Accuracy estimation of two global burned area products at national scale. In *IOP Conference Series: Earth and Environmental Science*; IOP Publishing Ltd: Bristol, UK, 2021; Volume 932. [CrossRef]
59. Grillakis, M.; Voulgarakis, A.; Rovithakis, A.; Seiradakis, K.D.; Koutroulis, A.; Field, R.D.; Kasoar, M.; Papadopoulos, A.; Lazaridis, M. Climate drivers of global wildfire burned area. *Environ. Res. Lett.* **2022**, *17*, 045021. [CrossRef]
60. Loudermilk, E.L.; O'Brien, J.J.; Goodrick, S.L.; Linn, R.R.; Skowronski, N.S.; Hiers, J.K. Vegetation's influence on fire behavior goes beyond just being fuel. *Fire Ecol.* **2022**, *18*, 9. [CrossRef]
61. Povak, N.A.; Hessburg, P.F.; Salter, R.B. Evidence for scale-dependent topographic controls on wildfire spread. *Ecosphere* **2018**, *9*, e02443. [CrossRef]
62. Beven, K.J.; Kirkby, M.J. A physically based, variable contributing area model of basin hydrology/Un modèle à base physique de zone d'appel variable de l'hydrologie du bassin versant. *Hydrol. Sci. J.* **1979**, *24*, 43–69. [CrossRef]
63. Weiss, A. Topographic position and landforms analysis. In Proceedings of the Poster Presentation, ESRI User Conference, San Diego, CA, USA, 9–13 July 2001.
64. Gorelick, N.; Hancher, M.; Dixon, M.; Ilyushchenko, S.; Thau, D.; Moore, R. Google Earth Engine: Planetary-scale geospatial analysis for everyone. *Remote Sens. Environ.* **2017**, *202*, 18–27. [CrossRef]

65. Reilley, C.; Crandall, M.S.; Kline, J.D.; Kim, J.B.; de Diego, J. The Influence of Socioeconomic Factors on Human Wildfire Ignitions in the Pacific Northwest, USA. *Fire* **2023**, *6*, 300. [CrossRef]
66. Li, H.; Vulova, S.; Rocha, A.D.; Kleinschmit, B. Exploring the monthly contribution of drivers on European summer wildfires with explainable artificial intelligence (XAI). *Ecol. Indic.* **2025**, *176*, 113605. [CrossRef]
67. Xu, Q.; Li, W.; Liu, J.; Wang, X. A geographical similarity-based sampling method of non-fire point data for spatial prediction of forest fires. *For. Ecosyst.* **2023**, *10*, 100104. [CrossRef]
68. Jiang, R.; Zhang, J. Leveraging Adaboost and Bayesian Optimization to Enhance Decision Tree Models for Wildfire Prediction. In *IGARSS 2025—2025 IEEE International Geoscience and Remote Sensing Symposium*; IEEE: New York City, NY, USA, 2025; pp. 237–240. [CrossRef]
69. Zhu, Z.; Deng, X.; Zhao, F.; Li, S.; Wang, L. How Environmental Factors Affect Forest Fire Occurrence in Yunnan Forest Region. *Forests* **2022**, *13*, 1392. [CrossRef]
70. Si, L.; Shu, L.; Wang, M.; Zhao, F.; Chen, F.; Li, W.; Li, W. Study on forest fire danger prediction in plateau mountainous forest area. *Nat. Hazards Res.* **2022**, *2*, 25–32. [CrossRef]
71. Chang, Y.; Zhu, Z.; Bu, R.; Chen, H.; Feng, Y.; Li, Y.; Hu, Y.; Wang, Z. Predicting fire occurrence patterns with logistic regression in Heilongjiang Province, China. *Landsc. Ecol.* **2013**, *28*, 1989–2004. [CrossRef]
72. Breiman, L. Random Forests. *Mach. Learn.* **2001**, *45*, 5–32. [CrossRef]
73. Cutler, D.R.; Edwards, T.C., Jr.; Beard, K.H.; Cutler, A.; Hess, K.T.; Gibson, J.; Lawler, J.J. Random Forests for Classification in Ecology. *Ecology* **2007**, *88*, 2783–2792. [CrossRef]
74. Iban, M.C.; Aksu, O. SHAP-Driven Explainable Artificial Intelligence Framework for Wildfire Susceptibility Mapping Using MODIS Active Fire Pixels: An In-Depth Interpretation of Contributing Factors in Izmir, Türkiye. *Remote Sens.* **2024**, *16*, 2842. [CrossRef]
75. Sandha, S.S.; Aggarwal, M.; Fedorov, I.; Srivastava, M. Mango: A Python Library for Parallel Hyperparameter Tuning. In *ICASSP 2020—2020 IEEE International Conference on Acoustics, Speech and Signal Processing (ICASSP)*; IEEE: New York City, NY, USA, 2020; pp. 3987–3991. [CrossRef]
76. Altmann, A.; Toloşi, L.; Sander, O.; Lengauer, T. Permutation importance: A corrected feature importance measure. *Bioinformatics* **2010**, *26*, 1340–1347. [CrossRef]
77. Janitza, S.; Strobl, C.; Boulesteix, A.-L. An AUC-based permutation variable importance measure for random forests. *BMC Bioinform.* **2013**, *14*, 119. [CrossRef]
78. Friedman, J.H. Greedy function approximation: A gradient boosting machine. *Ann. Stat.* **2001**, *29*, 1189–1232. [CrossRef]
79. Yeh, A.; Ngo, A. Bringing a Ruler Into the Black Box: Uncovering Feature Impact from Individual Conditional Expectation Plots. In *Machine Learning and Principles and Practice of Knowledge Discovery in Databases*; Springer: Cham, Switzerland, 2021; pp. 34–48. [CrossRef]
80. Jiménez-Valverde, A. Threshold-dependence as a desirable attribute for discrimination assessment: Implications for the evaluation of species distribution models. *Biodivers. Conserv.* **2014**, *23*, 369–385. [CrossRef]
81. Vien, B.; Wong, L.; Kuen, T.; Chiu, W.; Rose, L.R.F. A Machine Learning Approach for Anaerobic Reactor Performance Prediction Using Long Short-Term Memory Recurrent Neural Network. *Mater. Res. Proc.* **2021**, *18*, 61–70. [CrossRef]
82. Zhou, Q.; Qu, S.; Wang, Q.; She, Y.; Yu, Y.; Bi, J. Sliding Window-Based Machine Learning for Environmental Inspection Resource Allocation. *Environ. Sci. Technol.* **2023**, *57*, 16743–16754. [CrossRef]
83. Li, F.; Zhu, Q.; Yuan, K.; Ji, F.; Paul, A.; Lee, P.; Radeloff, V.C.; Chen, M. Projecting Large Fires in the Western US With an Interpretable and Accurate Hybrid Machine Learning Method. *Earth's Future* **2024**, *12*, e2024EF004588. [CrossRef]
84. Li, W.; Li, P.; Feng, Z. Delineating Fire-Hazardous Areas and Fire-Induced Patterns Based on Visible Infrared Imaging Radiometer Suite (VIIRS) Active Fires in Northeast China. *Remote Sens.* **2022**, *14*, 5115. [CrossRef]
85. Li, R.; Fu, Y.; Bergeron, Y.; Valeria, O.; Chavardès, R.D.; Hu, J.; Wang, Y.; Duan, J.; Li, D.; Cheng, Y. Assessing forest fire properties in Northeastern Asia and Southern China with satellite microwave Emissivity Difference Vegetation Index (EDVI). *ISPRS J. Photogramm. Remote Sens.* **2022**, *183*, 54–65. [CrossRef]
86. Masinda, M.M.; Li, F.; Qi, L.; Sun, L.; Hu, T. Forest fire risk estimation in a typical temperate forest in Northeastern China using the Canadian forest fire weather index: Case study in autumn 2019 and 2020. *Nat. Hazards* **2022**, *111*, 1085–1101. [CrossRef]
87. Fan, J.; Hu, T.; Ren, J.; Liu, Q.; Sun, L. A comparison of five models in predicting surface dead fine fuel moisture content of typical forests in Northeast China. *Front. For. Glob. Change* **2023**, *6*, 1122087. [CrossRef]
88. Su, Z.; Hu, H.; Tigabu, M.; Wang, G.; Zeng, A.; Guo, F. Geographically Weighted Negative Binomial Regression Model Predicts Wildfire Occurrence in the Great Xing'an Mountains Better Than Negative Binomial Model. *Forests* **2019**, *10*, 377. [CrossRef]
89. Fang, L.; Yang, J.; White, M.; Liu, Z. Predicting Potential Fire Severity Using Vegetation, Topography and Surface Moisture Availability in a Eurasian Boreal Forest Landscape. *Forests* **2018**, *9*, 130. [CrossRef]

90. Kampf, S.K.; Stevens-Rumann, C.S.; Nunes, L.; Sequeira, A.C.; Rego, F.C.; Fernández, C.; Hernández-Duarte, A.; Mosso, C.E.; Francois, J.P.; Miranda, A. Fire, Fuel, and Climate Interactions in Temperate Climates. *AGU Adv.* **2025**, *6*, e2024AV001628. [CrossRef]
91. Kim, E.-J.; Lee, S.-W. Structural Equation Model for Burn Severity with Topographic Variables and Susceptible Forest Cover. *Sustainability* **2018**, *10*, 2473. [CrossRef]
92. Adámek, M.; Jankovská, Z.; Hadincová, V.; Kula, E.; Wild, J. Drivers of forest fire occurrence in the cultural landscape of Central Europe. *Landsc. Ecol.* **2018**, *33*, 2031–2045. [CrossRef]
93. Zahura, F.T.; Bisht, G.; Li, Z.; McKnight, S.; Chen, X. Impact of topography and climate on post-fire vegetation recovery across different burn severity and land cover types through random forest. *Ecol. Inform.* **2024**, *82*, 102757. [CrossRef]
94. Cavieres, L.A.; Llambí, L.D.; Anthelme, F.; Hofstede, R.; Arroyo, M.T.K. High-Andean Vegetation Under Environmental Change: A Continental Synthesis. *Annu. Rev. Environ. Resour.* **2025**, *50*, 219–245. [CrossRef]
95. Yang, X.; Yao, C.; Chen, Q.; Ye, T.; Jin, C. Improved Estimates of Population Exposure in Low-Elevation Coastal Zones of China. *Int. J. Environ. Res. Public Health* **2019**, *16*, 4012. [CrossRef]
96. Masrur, A.; Taylor, A.; Harris, L.; Barnes, J.; Petrov, A. Topography, Climate and Fire History Regulate Wildfire Activity in the Alaskan Tundra. *J. Geophys. Res. Biogeosci.* **2022**, *127*, e2021JG006608. [CrossRef]
97. Alizadeh, M.R.; Abatzoglou, J.T.; Adamowski, J.; Modaresi Rad, A.; AghaKouchak, A.; Pausata, F.S.R.; Sadegh, M. Elevation-dependent intensification of fire danger in the western United States. *Nat. Commun.* **2023**, *14*, 1773. [CrossRef] [PubMed]
98. Rogeau, M.-P.; Armstrong, G.W. Quantifying the effect of elevation and aspect on fire return intervals in the Canadian Rocky Mountains. *For. Ecol. Manag.* **2017**, *384*, 248–261. [CrossRef]
99. Ma, W.; Feng, Z.; Cheng, Z.; Chen, S.; Wang, F. Identifying Forest Fire Driving Factors and Related Impacts in China Using Random Forest Algorithm. *Forests* **2020**, *11*, 507. [CrossRef]
100. Sun, H.; Wang, W.J.; Liu, Z.; Zou, X.; Zhang, Z.; Ying, H.; Dong, Y.; Yang, R. The relative importance of driving factors of wildfire occurrence across climatic gradients in the Inner Mongolia, China. *Ecol. Indic.* **2021**, *131*, 108249. [CrossRef]
101. Rihan, W.; Zhao, J.; Zhang, H.; Guo, X.; Ying, H.; Deng, G.; Li, H. Wildfires on the Mongolian Plateau: Identifying Drivers and Spatial Distributions to Predict Wildfire Probability. *Remote Sens.* **2019**, *11*, 2361. [CrossRef]
102. Afshari, S.; Sarli, R.; Alchin, A.A.; Aliabad, O.G.; Moradi, F.; Saei, M.; Lomer, A.R.B.; Nasiri, V. Trend analysis and interactions between surface temperature and vegetation condition: Divergent responses across vegetation types. *Environ. Monit. Assess.* **2025**, *197*, 292. [CrossRef] [PubMed]
103. Hammond, W.M.; Williams, A.P.; Abatzoglou, J.T.; Adams, H.D.; Klein, T.; López, R.; Sáenz-Romero, C.; Hartmann, H.; Breshears, D.D.; Allen, C.D. Global field observations of tree die-off reveal hotter-drought fingerprint for Earth's forests. *Nat. Commun.* **2022**, *13*, 1761. [CrossRef]
104. Bradstock, R.A. A biogeographic model of fire regimes in Australia: Current and future implications. *Global Ecol. Biogeogr.* **2010**, *19*, 145–158. [CrossRef]
105. Nolan, R.H.; Boer, M.M.; Resco de Dios, V.; Caccamo, G.; Bradstock, R.A. Large-scale, dynamic transformations in fuel moisture drive wildfire activity across southeastern Australia. *Geophys. Res. Lett.* **2016**, *43*, 4229–4238. [CrossRef]
106. Boving, I.; Celebrezze, J.; Salladay, R.; Ramirez, A.; Anderegg, L.D.L.; Moritz, M. Live fuel moisture and water potential exhibit differing relationships with leaf-level flammability thresholds. *Funct. Ecol.* **2023**, *37*, 2770–2785. [CrossRef]
107. Xu, W.; Zhou, Q.; Ma, W.; Huang, Y. Analysis of the Spatial Distribution Pattern of Grassland Fire Susceptibility and Influencing Factors in Qinghai Province. *Appl. Sci.* **2025**, *15*, 3386. [CrossRef]
108. Hu, T.; Zhou, G. Drivers of lightning- and human-caused fire regimes in the Great Xing'an Mountains. *For. Ecol. Manag.* **2014**, *329*, 49–58. [CrossRef]
109. Wang, H.; Jin, B.; Zhang, K.; Aktar, S.; Song, Z. Effectiveness in Mitigating Forest Fire Ignition Sources: A Statistical Study Based on Fire Occurrence Data in China. *Fire* **2022**, *5*, 215. [CrossRef]
110. Dorph, A.; Marshall, E.; Parkins, K.A.; Penman, T.D. Modelling ignition probability for human- and lightning-caused wildfires in Victoria, Australia. *Nat. Hazards Earth Syst. Sci.* **2022**, *22*, 3487–3499. [CrossRef]
111. Parisien, M.-A.; Parks, S.A.; Krawchuk, M.A.; Flannigan, M.D.; Bowman, L.M.; Moritz, M.A. Scale-dependent controls on the area burned in the boreal forest of Canada, 1980–2005. *Ecol. Appl.* **2011**, *21*, 789–805. [CrossRef] [PubMed]

Disclaimer/Publisher's Note: The statements, opinions and data contained in all publications are solely those of the individual author(s) and contributor(s) and not of MDPI and/or the editor(s). MDPI and/or the editor(s) disclaim responsibility for any injury to people or property resulting from any ideas, methods, instructions or products referred to in the content.